Journal of Power Sources 242 (2013) 141–147

Contents lists available at SciVerse ScienceDirect

Journal of Power Sources

journal homepage: www.elsevier.com/locate/jpowsour

Pd doped three-dimensional porous Ni film supported on Ni foam and its high performance toward $NaBH_4$ electrooxidation

Kui Cheng, Dianxue Cao, Fan Yang, Dongming Zhang, Peng Yan, Jinling Yin, Guiling Wang*

Key Laboratory of Superlight Material and Surface Technology of Ministry of Education, College of Material Science and Chemical Engineering, Harbin Engineering University, Harbin 150001, China

HIGHLIGHTS

- A novel 3D Pd-porous Ni/Ni foam electrode is successfully fabricated.
- Pd is uniformly distributed on the surface of porous Ni film supported on Ni foam.
- The electrode exhibits high performance and good stability for $NaBH_4$ oxidation.

GRAPHICAL ABSTRACT

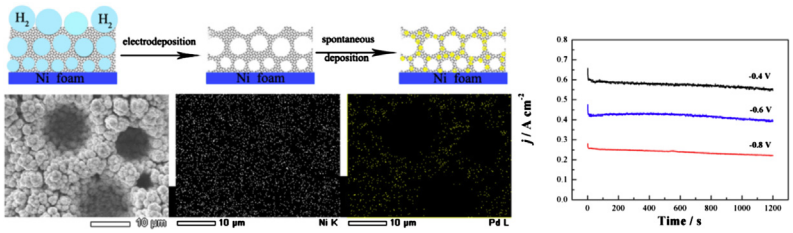

ARTICLE INFO

Article history:
Received 6 May 2013
Accepted 14 May 2013
Available online 28 May 2013

Keywords:
Palladium doped porous nickel film
Electrodeposition
Hydrogen template
Replacement reaction
Sodium borohydride electrooxidation

ABSTRACT

A novel three-dimensional electrode consisting of Pd doped porous Ni film supported on Ni foam (Pd-porous Ni/Ni) is successfully prepared. The porous Ni film is synthesized by electrodeposition of Ni nanoparticles using hydrogen bubbles as a dynamic template. Pd doping is carried out via a chemical replacement reaction between Ni film and Na_2PdCl_4 solution. The obtained electrode exhibits a three-dimensional (3D) porous structure allowing the full utilization of catalyst surface active sites. The morphology of the electrode and the distribution of Pd on Ni particle surfaces are characterized by scanning electron microscope and energy dispersive X-ray spectrometer. The structure is analyzed using an X-ray diffractometer. The catalytic performance of the porous 3D electrode is evaluated by voltammetry and chronoamperometry. Results show that the electrode displays high catalytic activity and good stability for $NaBH_4$ electrooxidation. The oxidation current density of $NaBH_4$ on the Pd-porous Ni/Ni in 3.0 mol L^{-1} NaOH containing 0.1 mol L^{-1} $NaBH_4$ at −0.6 V reaches 2.2 A mg^{-1}, which is about 22 times of that on Pd/C (0.1 A mg^{-1}) reported previously.

1. Introduction

Direct borohydride fuel cell (DBFC) is currently under investigation as a sustainable power source. Compared to other types of fuel cells, DBFC possesses several advantages, such as the high cell voltage (1.64 V employing oxygen as the oxidant and 2.11 V using H_2O_2 as the oxidant) and the high specific capacity (5.7 Ah g^{-1}). Besides, sodium borohydride fuel is non-combustible, non-toxic, safe, chemically stable, easy to store and transport in its dry state. It also has high hydrogen content (weight content of 10.6%). Therefore DBFC is regarded as a power generator having potential applications in mobile and portable electronic devices [1–6].

$NaBH_4$ directly electrooxidation (Eq. (1)) is usually accompanied by its hydrolysis reaction (Eq. (2)). Careful selections of the anode electrocatalysts of DBFC are crucial for improving DBFC performance. Ideal anode electrocatalysts should have high catalytic activity and stability for borohydride direct electrooxidation (Eq. (1)) and no catalytic activity for borohydride hydrolysis reaction (Eq. (2)), thus high fuel utilization and high cell performance can be realized [7,8].

* Corresponding author. Tel./fax: +86 451 82589036.
E-mail address: wangguiling@hrbeu.edu.cn (G. Wang).

0378-7753/$ – see front matter © 2013 Elsevier B.V. All rights reserved.
http://dx.doi.org/10.1016/j.jpowsour.2013.05.070

$$BH_4^- + 8OH^- \rightarrow BO_2^- + 4H_2O + 8e^- \quad (1)$$

$$NaBH_4 + 2H_2O \rightarrow 4H_2 + NaBO_2 \quad (2)$$

Noble metals exhibited higher catalytic activity than hydrogen storage alloys for $NaBH_4$ electrooxidation. However, they increased the cost of DBFC system. Therefore, enhancing the utilization efficiency of noble metal electrocatalysts to reduce their amount in DBFC is a hot topic in studies of DBFC [9–16]. Furthermore, electrode structures also remarkably influenced the catalytic performance of borohydride electrooxidation because the H_2 gas, if generated by hydrolysis, has to quickly diffuse away from the electrode, preventing surface active sites from blocking by adsorbed gas bubbles. In recent years, 3D porous nanosized metal films prepared by a hydrogen bubble template have elicited much attention due to their distinctive structural features and intriguing properties [17–22]. Various morphologies, such as dendrites, foam, honeycomb, and dish-like structures were prepared. These 3D porous nanosized metal films show high surface areas and open porous structures.

In this paper, we reported a 3D electrode with open structure for borohydride electrooxidation aiming to significantly improve the utilization of precious Pd catalyst. We chose Ni foam as the substrate due to its high electrical conductivity and a desirable open 3D structure. A 3D porous Ni particle layer was electrodeposited on Ni foam using hydrogen bubbles as a template to increase the surface area of Ni foam substrate. Pd was then deposited on Ni film surfaces by a simple chemical replacement reaction. The obtained 3D Pd-porous Ni/Ni foam electrode exhibited high catalytic performance and good stability for electrooxidation of $NaBH_4$.

2. Experimental

2.1. Preparation and characterization of Pd-porous Ni/Ni foam electrode

The schematic illustration for the preparation of the Pd-porous Ni/Ni foam electrode is shown in Scheme 1. The first step is the electrodeposition of porous Ni film on Ni foam. The second step is the deposition of Pd via a replacement reaction between Ni and Pd. The first step was carried out in the solution of 2.0 mol L^{-1} NH_4Cl + 0.1 mol L^{-1} $NiCl_2$ at a constant current of −2.0 A cm^{-2} for 100 s. The second step was performed by immersing the Ni/Ni-foam electrode in 1.0 mmol L^{-1} Na_2PdCl_4 solution for 1 min. Prior to use, the Ni foam (10 mm × 10 mm × 1.1 mm, 110 PPI, 320 g m^{-2}; Changsha Lyrun Material Co., Ltd. China) was degreased with acetone, etched with 6.0 mol L^{-1} HCl for 5 min, and then rinsed with deionized water extensively. The depositions were carried out in a three-electrode electrochemical cell controlled by computerized potentiostat (Autolab PGSTAT302, Eco Chemie). The Ni foam served as the working electrode, which was placed between two pieces of platinum foil in parallel as the counter electrodes. A saturated Ag/AgCl, KCl_{std} electrode was used as the reference electrode.

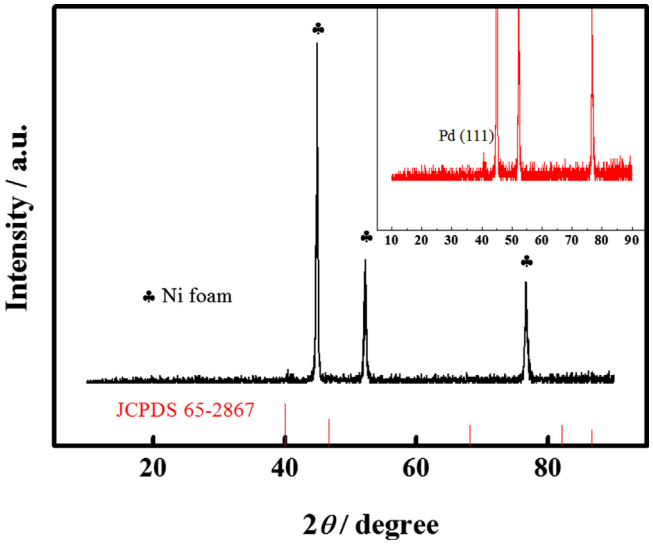

Fig. 1. The XRD pattern of the Pd-porous Ni/Ni foam electrode. The insert is the zoom of the diffraction peak area of the Pd.

The electrode morphology was characterized by a scanning electron microscope (SEM, JEOL JSM-6480) equipped with an energy dispersive X-ray spectrometer (EDX). The structure was analyzed using an X-ray diffractometer (Rigaku TTR III) with Cu Kα radiation (λ = 0.1514178 nm). The Pd loading was measured using an inductive coupled plasma emission spectrometer (ICP, Xseries II, Thermo Scientific). Pd in the 1.0 cm^2 electrode was first dissolved in aqua regia solution and then diluted to 1 L solution for the ICP measurement.

2.2. Electrochemical measurements

The catalytic performance of the Pd-porous Ni/Ni foam electrode for $NaBH_4$ electrooxidation was measured by linear scan voltammetry and chronoamperometry in a standard three-electrode electrochemical cell with Ag/AgCl, KCl_{std} reference electrode and Pt foil counter electrode. The electrolyte is NaOH solution. The reported current densities were calculated using the geometrical area of the electrode. All solutions were made with analytical grade chemical reagents and ultra-pure water (Milli-Q 18 MΩ cm). All potentials were referred to the Ag/AgCl, KCl_{std} reference electrode. All measurements were performed at room temperature (25 ± 1 °C) and all the electrolytes were deoxygenated by N_2 bubbling.

3. Results and discussion

3.1. Characterization of Pd-porous Ni/Ni foam electrode

Fig. 1 shows the XRD pattern of the 3D Pd-porous Ni/Ni foam electrode. The three diffraction peaks at 44.5°, 51.8° and 76.3° can

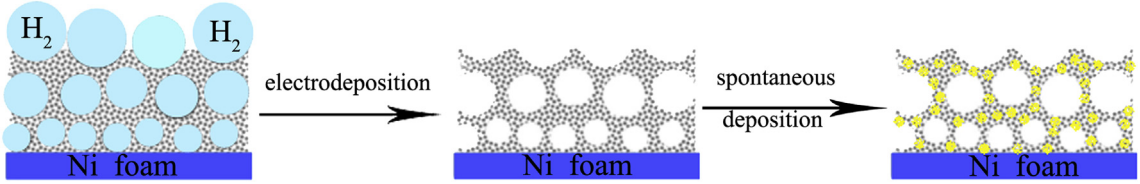

Scheme 1. Schematic diagram for the preparation of the Pd-porous Ni/Ni foam electrode.

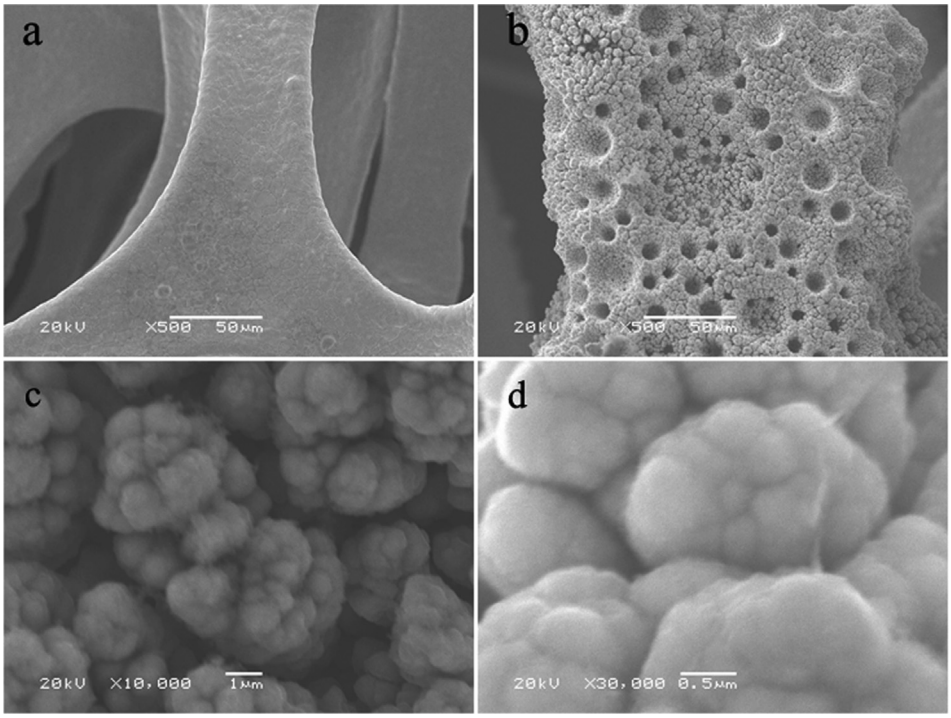

Fig. 2. SEM images of the Ni foam (a), porous Ni/Ni foam (b) and Pd-porous Ni/Ni foam (c and d).

be indexed to the diffraction from the (111), (200) and (220) plane of Ni metal, respectively, according to the standard crystallographic spectrum of Ni (JCPDS card No. 40-0850). The insert of Fig. 1 shows the amplified XRD pattern, from which a peak at 40° can be clearly seen. This peak matched well with the (111) plane of Pd according to the standard crystallographic spectrum of Pd (JCPDS card No. 65-2867). The diffraction peak of Pd is much weaker than that of Ni suggesting that a small amount of Pd was deposited on porous Ni film.

Typical SEM images of the Ni foam substrate, the 3D porous Ni film and the Pd-porous Ni/Ni foam electrode are presented in Fig. 2. The Ni foam substrate showed a 3D network structure with micro

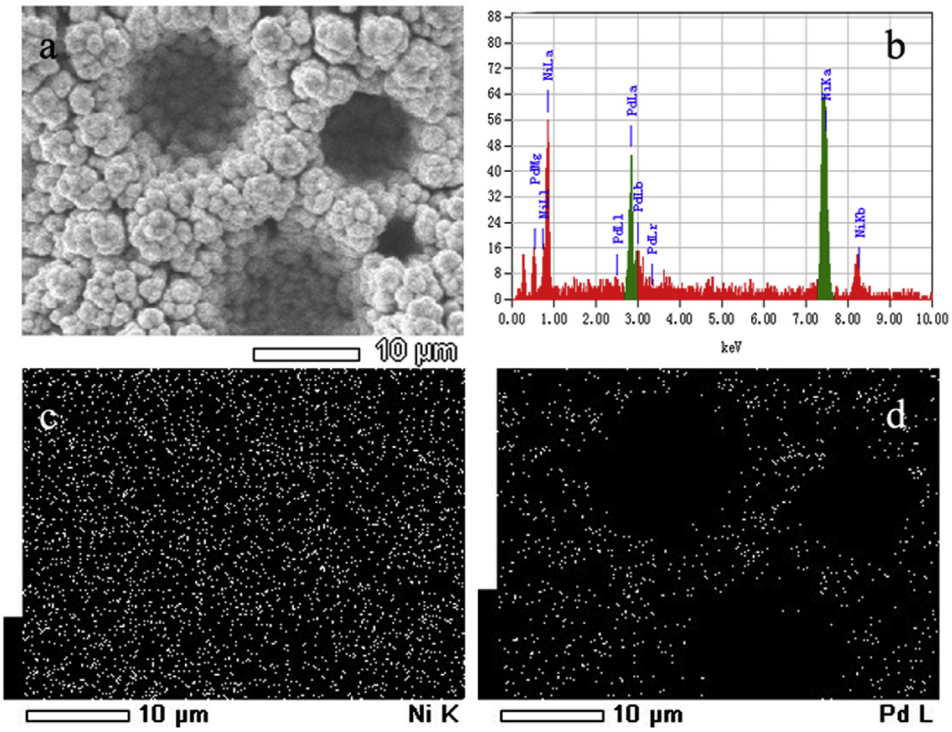

Fig. 3. The SEM image (a), the corresponding EDX spectrum (b) of the Pd-porous Ni/Ni foam electrode and the corresponding elemental distributions of Ni and Pd (c and d).

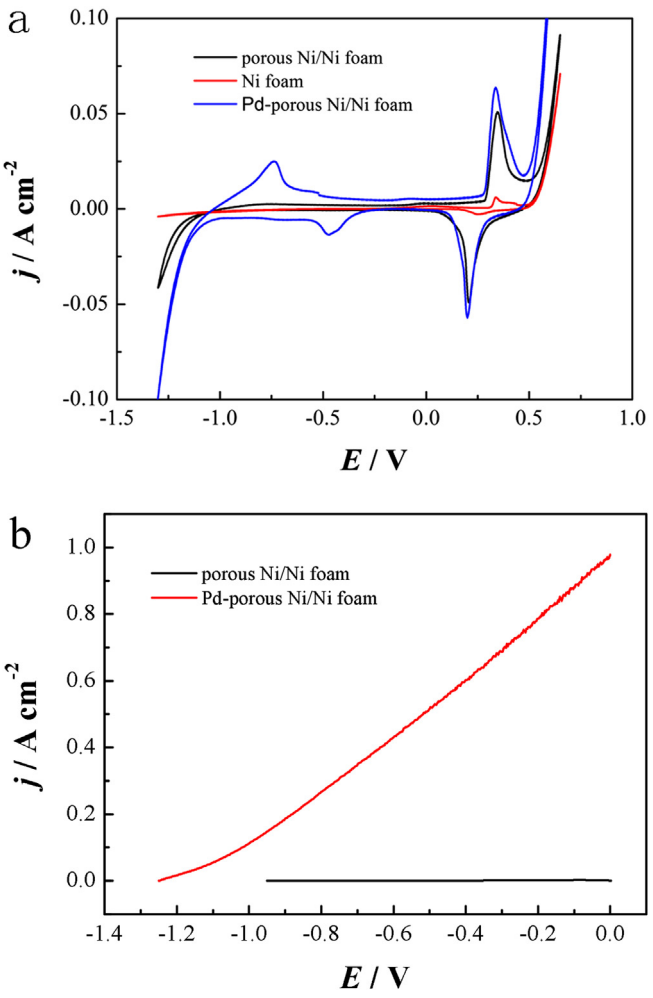

Fig. 4. Cyclic voltammograms of Ni foam, porous Ni/Ni foam and Pd-porous Ni/Ni foam electrodes in 3.0 mol L^{-1} NaOH at a scan rate of 50 mV s^{-1} (a). The comparative polarization curves of porous Ni/Ni foam and Pd-porous Ni/Ni foam in 3.0 mol L^{-1} NaOH + 0.1 mol L^{-1} $NaBH_4$ at 10 mV s^{-1}(b).

open cages and zigzag flow channels (Fig. 2a). After electrodeposition of Ni, the smooth surface of the skeleton of the Ni foam disappeared and the surface was uniformly covered with a highly porous Ni layer (Fig. 2b), which exhibited a 3D porous structure with typical large pores of 5–20 μm in diameter. The Ni film consisted of numerous interconnected nanoparticles with diameters of 200–300 nm. This unique structure of Ni film remarkably increased the surface area of Ni foam substrate and also provided a 3D porous skeleton for Pd spontaneous deposition. Fig. 2c and d shows that Pd was uniformly distributed on the surface of Ni nanoparticles after the spontaneous deposition and the surface of Ni particles became rough. The Pd surfaces can be fully utilized because all the Pd particles are accessible to $NaBH_4$ and electrolytes. Besides, hydrogen generated by $NaBH_4$ hydrolysis can quickly diffuse away from the electrode, preventing Pd active sites from blocking by adsorbed gas bubbles.

Fig. 3a and b shows the SEM image and the corresponding EDX spectrum of the Pd-porous Ni/Ni foam electrode, respectively. As seen from Fig. 3a, the 3D porous structure of the Ni/Ni foam substrate was well maintained after Pd replacement, Fig. 3b demonstrated that Pd was deposited on the Ni surfaces. Fig. 3c and d shows the Ni and Pd elemental mappings, respectively. It can be seen that Pd was uniformly distributed on the surface of porous Ni film and its content was clearly lower than Ni, which is in good agreements with the data from ICP measurements (0.1791 mg cm^{-2}).

3.2. Electrocatalytic performance of the Pd-porous Ni/Ni foam electrode for $NaBH_4$ oxidation

Catalytic performances are influenced strongly by the structure and surface composition of the electrode. Fig. 4a shows the cyclic voltammograms of the Ni foam, porous Ni/Ni foam and Pd-porous Ni/Ni foam electrodes measured in NaOH solution. Both the Ni foam and the 3D porous Ni/Ni foam showed an oxidation peak at around 0.34 V and a reduction peak at about 0.21 V. This couple of redox peaks can be attributed to the redox reaction between Ni(II)/Ni(III) in the alkaline electrolyte as shown by Eq. (3) [22].

$$Ni(OH)_2 + OH^- \Leftrightarrow NiOOH + H_2O + e^- \quad (3)$$

The porous Ni/Ni foam has a much larger peak area than Ni foam substrate due to its highly porous structure. The CV of Pd-porous Ni/Ni foam electrode exhibited a strong anodic peak centered at

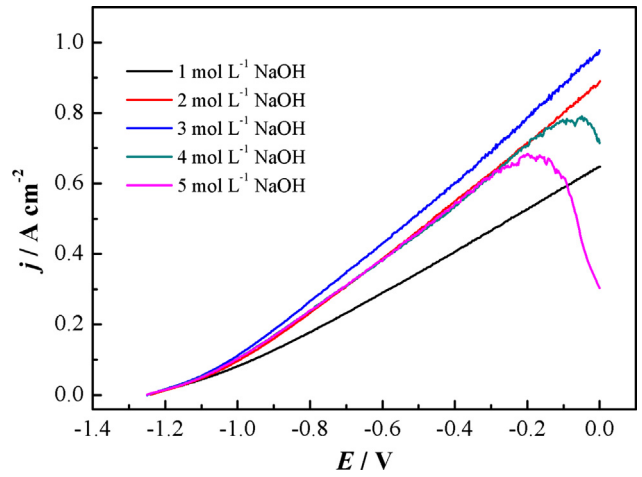

Fig. 5. Linear scan voltammograms of $NaBH_4$ electrooxidation at the Pd-porous Ni/Ni foam electrode in *x* mol L^{-1} NaOH (*x* = 1, 2, 3, 4, 5) + 0.1 mol L^{-1} $NaBH_4$. Scan rate: 10 mV s^{-1}.

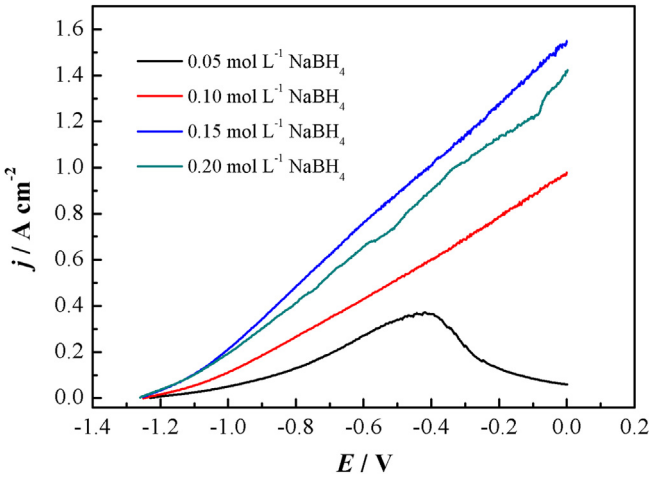

Fig. 6. Linear scan voltammograms of $NaBH_4$ electrooxidation at the Pd-porous Ni/Ni foam electrode in 3.0 mol L^{-1} NaOH + *x* mol L^{-1} $NaBH_4$ (*x* = 0.05, 0.10, 0.15, 0.20). Scan rate: 10 mV s^{-1}.

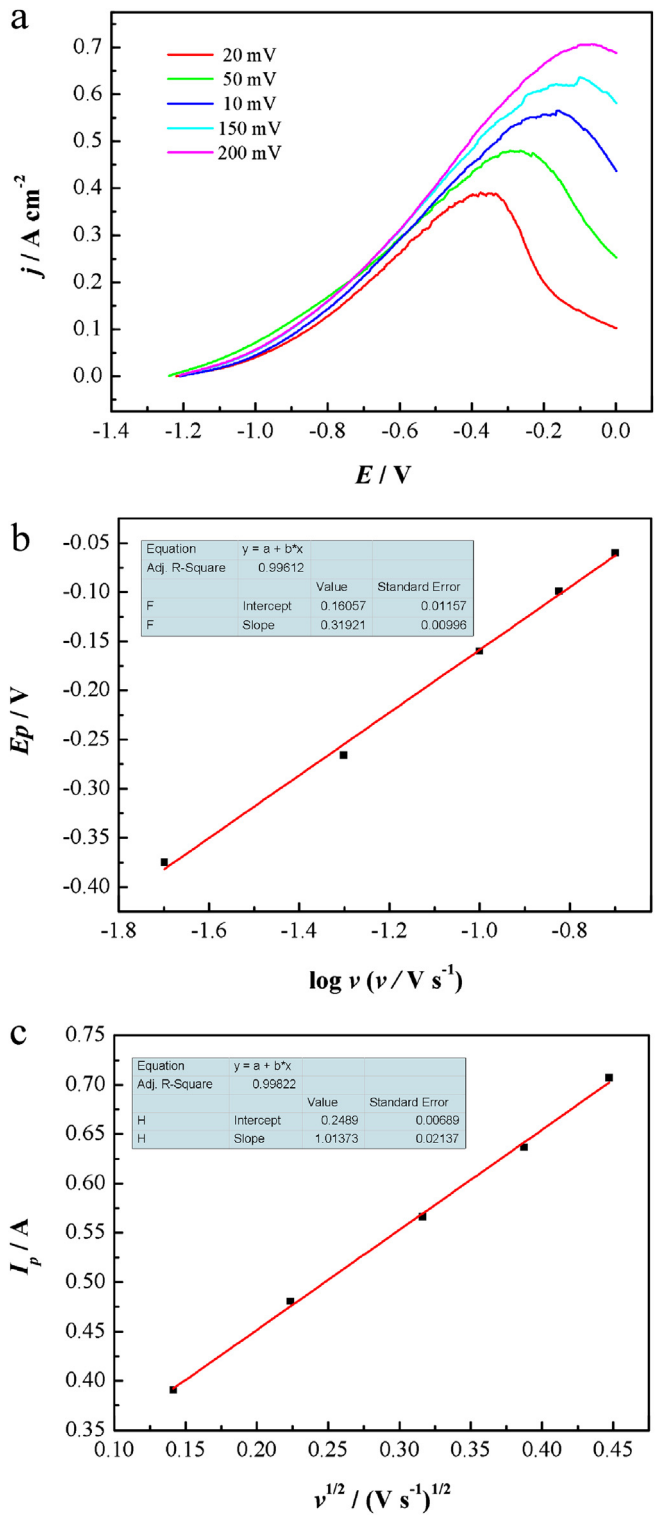

Fig. 7. Linear scan voltammograms of $NaBH_4$ electrooxidation at the Pd-porous Ni/Ni foam electrode in 3.0 mol L^{-1} KOH + 0.05 mol L^{-1} $NaBH_4$ at different scan rates (a), the plot of E_p vs. log v (b) and the plot of I_p vs. $v^{1/2}$ (c).

around −0.75 V corresponding to the electrooxidation of hydrogen on Pd surface. The cathodic peak at around −0.46 V can be attributed to the reduction Pd surface oxides. So the CV demonstrated that Pd was deposited on Ni film by replacement reaction. The charge obtained from the cathodic peak centered at −0.46 V was employed to estimate the electrochemically active surface areas (ECSAs) of Pd by assuming that a monolayer of PdO was formed and its reduction charge value is 405 μC cm^{-2} [23]. Such estimation gave an ECSAs of 106 cm^2. ICP measurement shows that the Pd loading is 0.1791 mg. So the specific ECSAs of Pd reached 59.2 m^2 g^{-1}, which is much larger than that reported in the previous work (21.4 m^2 g^{-1} and 40 m^2 g^{-1}) [24,25]. Ni foam is commonly chosen as an electrode substrate due to its high electrical conductivity, stable in alkaline electrolyte, and a desirable 3D macroporous structure [26–30]. The large ECSAs of Pd in the Pd-porous Ni/Ni foam electrode may be ascribed to the highly uniform dispersion of Pd on the porous Ni film surfaces. In addition, the current at −1.0 V on the Pd-porous Ni/Ni foam electrode is much larger than that of porous Ni film and Ni foam substrate, which revealed that the introduction of Pd could obviously enhance the ability of hydrogen absorption/desorption leading to higher activity of electrode. Fig. 4b shows the polarization curves of the porous Ni/Ni foam and Pd-porous Ni/Ni foam electrodes in 3.0 mol L^{-1} NaOH + 0.1 mol L^{-1} $NaBH_4$. Apparently, the Pd-porous Ni/Ni foam electrode, even with a very low Pd content, has a remarkably higher catalytic activity for $NaBH_4$ electrooxidation than the porous Ni/Ni foam electrode. The oxidation current density of 0.603 A cm^{-2} was achieved at −0.4 V in the solution of 3.0 mol L^{-1} NaOH + 0.1 mol L^{-1} $NaBH_4$ at the Pd-porous Ni/Ni foam electrode.

Effects of NaOH concentration on $NaBH_4$ electrooxidation at the Pd-porous Ni/Ni foam electrode were investigated and the results are presented in Fig. 5. The $NaBH_4$ electrooxidation activity increased with the increase of NaOH concentration from 1.0 to 3.0 mol L^{-1}. However, when the NaOH concentration is higher than 3.0 mol L^{-1}, the peak current decreased and the peak shifted toward a less negative potential. As known, the flux at the electrode surface is proportional to $CD^{1/2}$ (C: concentration, D: diffusion coefficient) [31]. When the $NaBH_4$ concentration remains the same, the flux ratio of $[OH^-]/[BH_4^-]$ increased with the increase of NaOH concentration. Since the reaction is controlled by $NaBH_4$ diffusion, the increase of $[OH^-]/[BH_4^-]$ causes the decrease of the oxidation current density and the shift of peak toward more negative potentials.

Fig. 6 shows the linear scan voltammograms (LSV) of $NaBH_4$ electrooxidation at the Pd–Ni/Ni foam electrode in 3.0 mol L^{-1} NaOH containing different concentrations of $NaBH_4$. The open circuit potential (OCP) for the $NaBH_4$ oxidation at the Pd-porous Ni/Ni foam electrode was around −1.2 V and shift to more negative values

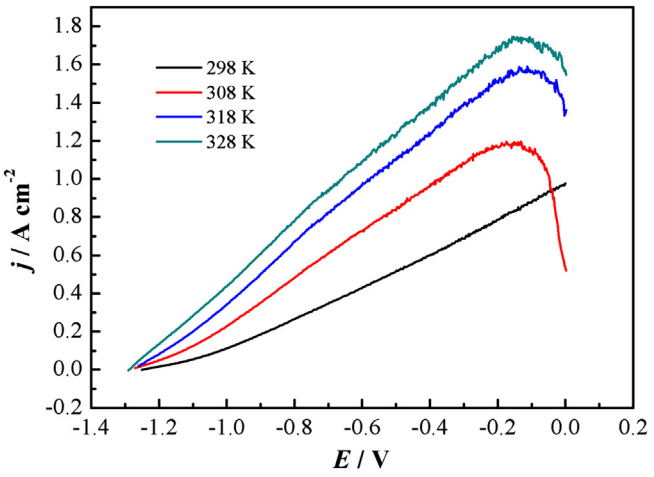

Fig. 8. Linear scan voltammograms of $NaBH_4$ electrooxidation at the Pd-porous Ni/Ni foam electrode in 3.0 mol L^{-1} KOH + 0.1 mol L^{-1} $NaBH_4$ at different temperatures. Scan rate: 10 mV s^{-1}.

with the increase of $NaBH_4$ concentration. The oxidation current density increased with $NaBH_4$ concentration up to 0.15 mol L^{-1}, suggesting that the reaction is controlled by the $NaBH_4$ diffusion. A further increase in the $NaBH_4$ concentration resulted in a decrease of current density, and gas bubbles were formed on the electrode surface by $NaBH_4$ hydrolysis, which blocked the $NaBH_4$ diffusion leading to current density decreases. So the ratio of $NaBH_4$ to NaOH concentration has significant effects on the performance of $NaBH_4$ electrooxidation at the Pd-porous Ni/Ni foam electrode.

The estimation of the total number of electrons exchanged (n) in the BH_4^- electrooxidation is important for the catalyst evaluation. For an irreversible anodic reaction, the peak potential E_p, peak current I_p and scan rate v have the following the relationship (Eqs. (4) and (5)) [32]:

$$E_p = E^{\theta'} + b\left[0.52 - \frac{1}{2}\log\left(\frac{b}{D}\right) - \log k^{\theta} + \frac{1}{2}\log v\right] \quad (4)$$

$$I_p = \left(3\times 10^5\right) n\left(\frac{2.3RT}{bF}\right)^{\frac{1}{2}} AC_b D^{\frac{1}{2}} v^{\frac{1}{2}} \quad (5)$$

Fig. 7 shows the LSV of $NaBH_4$ oxidation at the Pd-porous Ni/Ni foam electrode recorded at different scan rates in 3.0 mol L^{-1} NaOH + 0.05 mol L^{-1} $NaBH_4$. The potential of the oxidation peak shifted to more positive value with the increase of scan rate, demonstrating the irreversible nature of $NaBH_4$ electrooxidation reaction. Fig. 7b is the plot of E_p against $\log v^{1/2}$. The *Tafel* slope b can be obtained from the slope of the straight line according to Eq. (3), which was found to be 0.31921. Fig. 7c is the plot of the current density of the oxidation peak against the square root of scan rate. Clearly, the oxidation peak current density varied linearly with the square root of scan rates. This demonstrated that the electrooxidation of $NaBH_4$ on the Pd-porous Ni/Ni foam electrode is a diffusion-controlled process. From the slope of this straight line and b, the number of electron n can be estimated according to Eq. (4), which was found to be 6.6, much higher than the literature result [15]. This implies that that the Pd-porous Ni/Ni foam electrode could reduce hydrogen evolution and increase utilization efficiency of the fuel.

The effect of temperature on the electrocatalytic activity of $NaBH_4$ oxidation at the Pd-porous Ni/Ni foam electrode was also investigated. Higher temperature usually results in faster electrode kinetics [33]. Fig. 8 shows LSV of $NaBH_4$ electrooxidation at the Pd-porous Ni/Ni foam in 3.0 mol L^{-1} NaOH + 0.1 mol L^{-1} $NaBH_4$ at different temperatures. The performance of $NaBH_4$ electrooxidation improved remarkably by increasing the reaction temperature. When the temperature increased from 298 to 328 K, the oxidation current density at −0.6 V increased from 0.430 to 1.096 A cm^{-2}. However, high temperature also results in high rate of $NaBH_4$ hydrolysis, which could reduce the utilization of $NaBH_4$ fuel. Therefore, operating at low temperature is important for minimizing gas evolution and achieving high utilization of the reactants.

The stability of the Pd-porous Ni/Ni foam electrode for $NaBH_4$ electrooxidation was investigated by chronoamperometric measurements. Fig. 9 shows the chronoamperometric curves of $NaBH_4$ electrooxidation at the Pd-porous Ni/Ni foam electrode in the solution of 3.0 mol L^{-1} KOH + 0.1 mol L^{-1} $NaBH_4$. The oxidation currents reached a steady-state quickly after the potential was applied and slightly decreased within the test period at the three different potentials (−0.8, −0.6 and −0.4 V), indicating that the Pd-porous Ni/Ni foam electrode has a good stability for catalyzing the $NaBH_4$ electrooxidation. The current density after 1200 s reaction at −0.4, −0.6 and −0.8 V was 0.547, 0.395 and 0.221 A cm^{-2}, respectively. The stabilized mass current density at −0.6 V is 2.2 A mg^{-1}, which is about 22 times of that for Pd/C (0.1 A mg^{-1}) reported previously [34].

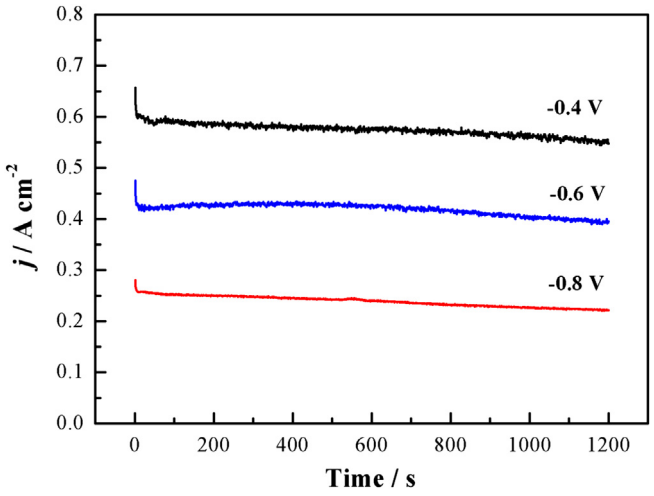

Fig. 9. Chronoamperometric curves for $NaBH_4$ electrooxidation at the Pd-porous Ni/Ni foam electrode at different potentials in 3.0 mol L^{-1} KOH + 0.1 mol L^{-1} $NaBH_4$.

4. Conclusion

A high performance 3D Pd-porous Ni/Ni foam electrode is successfully demonstrated. The porous 3D Ni film prepared by electrodeposition of Ni on the Ni foam substrate accompanying hydrogen evolution was found to be consisting of interconnected microparticles. The simple replacement reaction between the porous Ni film and Na_2PdCl_4 in solution successfully introduced highly dispersed Pd on the porous Ni film surfaces. The 3D porous electrode exhibited high catalytic performance and good stability for $NaBH_4$ electrooxidation. In the solution of 3.0 mol L^{-1} NaOH + 0.1 mol L^{-1} $NaBH_4$, the oxidation current density at −0.6 V (2.2 A mg^{-1}) is about 22 times higher than that for Pd/C (0.1 A mg^{-1}) reported previously. The enhanced performance is ascribed to the unique structure of electrode, which ensures high utilization of Pd nanoparticles and quick releases of gas bubbles produced by hydrolysis from the electrode. The novel Pd-porous Ni/Ni foam electrode has a great potential as the anode of DBFC due to its facile preparation, high performance and low cost.

Acknowledgments

We gratefully acknowledge the financial support of this research by Harbin Science and Technology Innovation Fund for Excellent Academic Leaders (2012RFXXG103) and Fundamental Research Funds for the Central Universities (HEUCFT1205).

References

[1] M. Jia, N.A. Choudhury, Y. Sahai, Renewable Sustainable Energy Rev. 14 (2010) 183–199.
[2] J. Ma, N.A. Choudhury, Y. Sahai, Renewable Sustainable Energy Rev. 14 (2010) 183–199.
[3] D.M.F. Santos, C.A.C. Sequeira, Renewable Sustainable Energy Rev. 15 (2011) 3980–4001.
[4] J.-H. Wee, J. Power Sources 161 (2006) 1–10.
[5] J.H. Wee, J. Power Sources 155 (2006) 329–339.
[6] Y. Wang, P. He, H. Zhou, Energy Environ. Sci. 3 (2010) 1515–1518.
[7] U.B. Demirci, J. Power Sources 172 (2007) 676–687.
[8] B.H. Liu, Z.P. Li, J. Power Sources 187 (2009) 291–297.
[9] D. Cao, Y. Gao, G. Wang, R. Miao, Y. Liu, Int. J. Hydrogen Energy 35 (2010) 807–813.
[10] K. Cheng, D. Cao, F. Yang, L. Zhang, Y. Xu, G. Wang, J. Mater. Chem. 22 (2012) 850–855.

[11] K. Cheng, Y. Xu, R.R. Miao, F. Yang, J.L. Yin, G.L. Wang, D.X. Cao, Fuel Cells 12 (2012) 869–875.
[12] G.-j. Wang, Y.-z. Gao, Z.-b. Wang, C.-y. Du, J.-j. Wang, G.-p. Yin, J. Power Sources 195 (2010) 185–189.
[13] L. Yi, B. Hu, Y. Song, X. Wang, G. Zou, W. Yi, J. Power Sources 196 (2011) 9924–9930.
[14] L. Yi, L. Liu, X. Wang, X. Liu, W. Yi, X. Wang, J. Power Sources 224 (2013) 6–12.
[15] J.Q. Yang, B.H. Liu, S. Wu, J. Power Sources 194 (2009) 824–829.
[16] V.W.S. Lam, D.C.W. Kannangara, A. Alfantazi, E.L. Gyenge, J. Power Sources 212 (2012) 57–65.
[17] I. Herraiz-Cardona, E. Ortega, L. Vázquez-Gómez, V. Pérez-Herranz, Int. J. Hydrogen Energy 37 (2012) 2147–2156.
[18] D. Hua, C. Xiaodong, J. Phys. Chem. C 113 (2009) 603–609.
[19] Y. Li, Y.-Y. Song, C. Yang, X.-H. Xia, Electrochem. Commun. 9 (2007) 981–988.
[20] H.C. Shin, J. Dong, M. Liu, Adv. Mater. 15 (2003) 1610–1614.
[21] H.-C. Shin, M. Liu, Chem. Mater. 16 (2004) 5460–5464.
[22] W. Xing, S. Qiao, X. Wu, X. Gao, J. Zhou, S. Zhuo, S.B. Hartono, D. Hulicova-Jurcakova, J. Power Sources 196 (2011) 4123–4127.
[23] T. Chierchie, C. Mayer, W.J. Lorenz, J. Electroanal. Chem. Interfacial Electrochem. 135 (1982) 211–220.
[24] R. Rego, C. Oliveira, A. Velázquez, P.-L. Cabot, Electrochem. Commun. 12 (2010) 745–748.
[25] C. Hu, Z. Bai, L. Yang, J. Lv, K. Wang, Y. Guo, Y. Cao, J. zhou, Electrochim. Acta 55 (2010) 6036–6041.
[26] R.-Y. Ji, D.-S. Chan, J.-J. Jow, M.-S. Wu, Electrochem. Commun. 29 (2013) 21–24.
[27] C. Celik, F.G. Boyaci San, H.I. Sarac, Fuel Cells 12 (2012) 1027–1031.
[28] T.K. Kim, W. Chen, C. Wang, J. Power Sources 196 (2011) 8742–8746.
[29] J. Liu, Y. Feng, X. Wang, Q. Yang, X. Shi, Y. Qu, N. Ren, J. Power Sources 198 (2012) 100–104.
[30] W. Yang, S. Yang, W. Sun, G. Sun, Q. Xin, J. Power Sources 160 (2006) 1420–1424.
[31] B.H. Liu, J.Q. Yang, Z.P. Li, Int. J. Hydrogen Energy 34 (2009) 9436–9443.
[32] E. Gyenge, Electrochim. Acta 49 (2004) 965–978.
[33] E. Hao Yu, K. Scott, R.W. Reeve, J. Electroanal. Chem. 547 (2003) 17–24.
[34] B.H. Liu, Z.P. Li, S. Suda, Electrochim. Acta 49 (2004) 3097–3105.